

Table of Contents

1. Research Methodology	2
1.1 Reactor configurations and experimental set-up	2
1.2 Analytical procedure.....	5
2. Key Findings.....	8
2.1 Electrochemical oxidation of DCF.....	8
2.2 Effect of the applied current density and reaction kinetics	9
2.3 Effect of electrolyte composition: sulfate to chloride ratio.....	11
2.4 Effect of electrode material.....	15
2.5 Phytotoxicity study	18
2.6 Comparative study of EC alone, PMS alone, EC/PMS, and Fe ₂ SO ₄ /PMS...	19
2.7 Results of response surface methodology	23
2.8 Performance in continuous flow mode.....	27
2.9 Results of LC-MS analysis	30
3. Conclusion.....	32
References	34

1. Research Methodology

1.1 Reactor configurations and experimental set-up

Outline of experimental work is given in Figure 1. All experiments were conducted in an undivided cell made up of acrylic and having dimensions: 200 mm x 120 mm x 70 mm. Experiments were performed at least twice to ensure the accuracy of data.

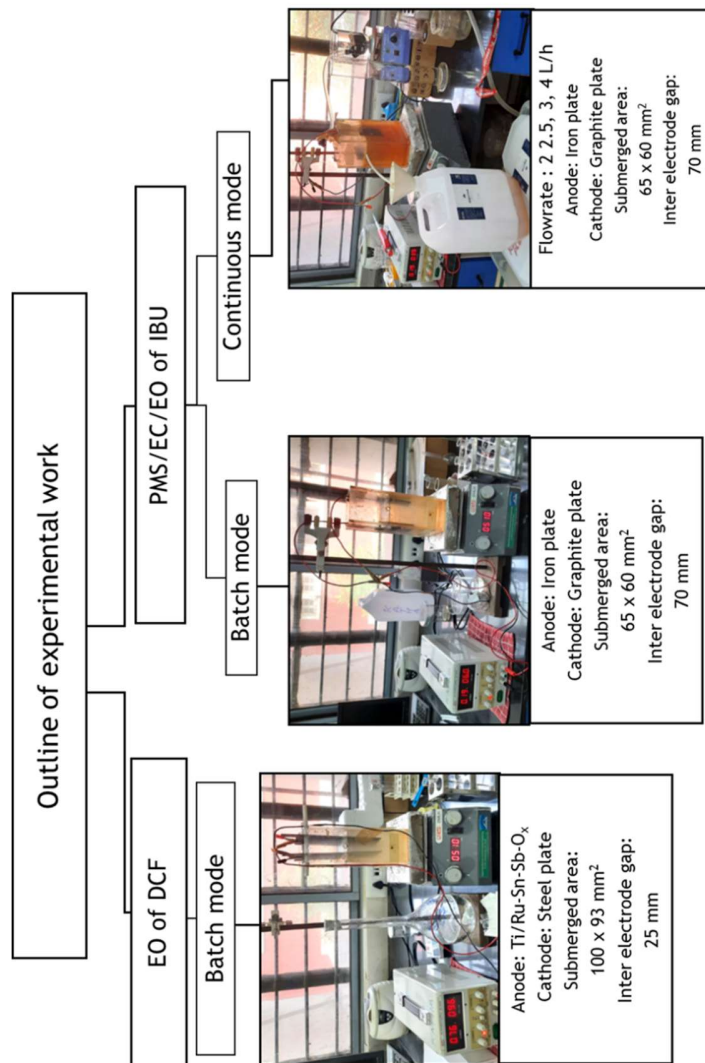


Figure 1: Outline of the experimental work carried out in the present study

ECO experiments: Electrodes were placed 40 mm apart on grooved Teflon spacers. The DSA (dimensionally stable anode) was prepared indigenously using the thermal decomposition method (Soni et al., 2020). Titanium plate (90% pure, Unisys Ortho., Ahmedabad) was base metal, its surface was roughened with silicon carbide paper and plate was etched in 10% oxalic acid for 1 hour at 80⁰ C. The precursor solution was prepared from RuCl₃, SnCl₂, and SbCl₃ salts, in IPA and 37% HCl solution. The freshly prepared precursor solution was applied on the titanium plate simply by brush. The solvent was allowed to dry for 5 minutes at room temperature and then it was oven-dried for 5 minutes at 80⁰C to ensure solvent evaporation. It was then heated at 550⁰C for 5 minutes to ensure the calcination of metallic salts. These steps ‘applying precursor-drying-evaporating-calcination’ were repeated after each coating for 15 to 16 times. After 15-16 coats of precursor solution, the plate achieved 1.5 mg/cm² weight gain, which ensured mixed metal coating. Then the plate was heated in a muffle furnace for 1 h to fix the film of metal oxides. The mol ratio of Ru:Sn:Sb in the coating was kept at 1:4:0.67. A steel plate was used as a cathode. The effective area (exposed to the solution) of electrodes was 100 mm x 93 mm. Electrochemical oxidation was performed in a batch mode. The current densities 5, 7.5, and 10 mA/cm²; were applied and controlled galvano-statically by DC power supply (HTC instruments, Mumbai; range: 0-1 A and 0-30 V). All experiments were performed at neutral pH (7.5 to 7.8) and no further pH adjustment was done. The temperature was maintained at 27±2 °C throughout the experiments. Solution volume was 1 L, prepared by spiking diclofenac sodium (200 ppm in stock solution) in distilled water or RO concentrate to achieve 10 ppm DCF concentration. It was continuously stirred at 500 rpm. To check the effect of sulphate to chloride ratio, sodium sulphate and sodium chloride were added in distilled water so as to adjust sulphate to chloride mass ratios of S:C = 0.6:1, 0.85:1, 1.1:1, 1.35:1, and 1.6:1; keeping total dissolved solids 1000 mg/L. To avoid the effect of total salt concentration, these matrices were synthesized in such a way that total salt concentration remained 1000 mg/L. All the experiments were carried out at least twice.

EC/PMS experiments: The iron plate was used as a sacrificial anode and graphite plate was used as a cathode having dimensions 11 cm x 8 cm x 0.5 cm. Electrodes were placed

70 mm apart. The effective area of electrodes exposed to the solution was 9.5 cm x 8 cm. Experiments were carried out in batch mode as well as continuous mode. The temperature was maintained at 27 ± 2 °C throughout the experiments. **Batch experiments:** At the start, 1 L of ROC spiked with 10 mg/L IBU was added in the acrylic cell. The cell was placed on the stirrer plate and the solution was stirred with a magnetic bar at 500 rpm. An initial sample was withdrawn and a predetermined amount of PMS was then added in the cell, at the same time current was supplied to start the reaction. DC power supply (HTC instruments, Mumbai; range: 0-1 A and 0-30 V) was used to apply and control current density. The reaction time for all batch experiments was 30 min. Figure 2 shows the batch experimental set up. **Continuous flow experiments:** Reactor was run in batch mode for half an hour and then feed was started at controlled flow. Initially, experiments were carried out at 2 L/h flow rate which gives 30 min retention time. Later for optimization purposes, the flow rate was increased to 2.5 L/h, 3 L/h, and 4 L/h which give 24 min, 20 min, and 15 min respectively. Fifteen minutes buffer time was given to achieve steady-state condition and samples were started taken after this at every fifteen-minute for one hour and then the interval was increased to thirty minutes. Reactor was run in continuous mode for 3 h. Feed was stored in the reservoir which contained 10 mg/L IBU, 500 mg/L PMS dissolved in ROC. Feed was introduced at the bottom right corner as shown in Figure 3, and the outlet was on upper left side to ensure that there is no short circuit of flow. The effluent was collected directly from an outlet for analysis.

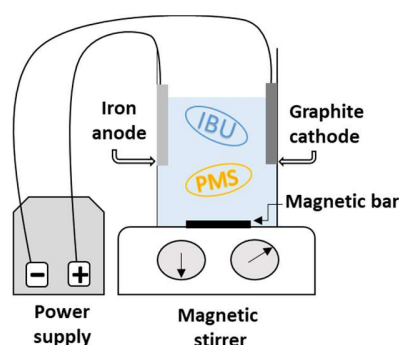


Figure 2: Schematic view of the batch experimental setup

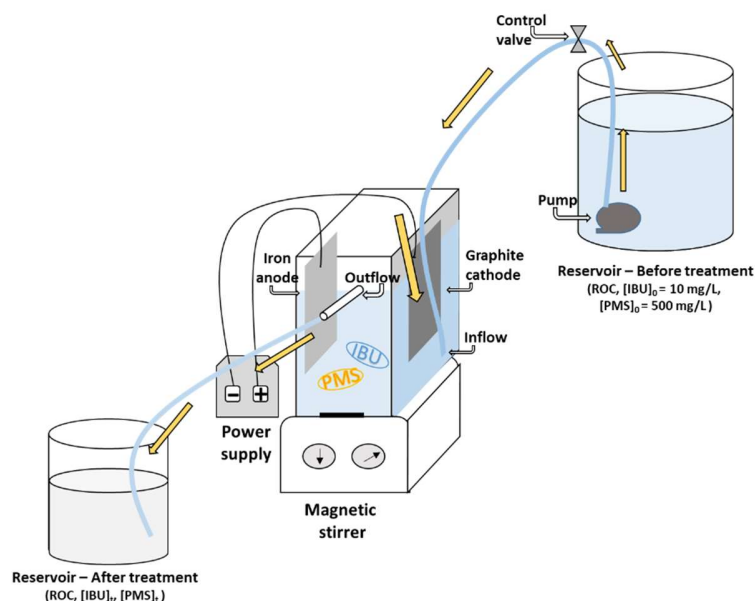


Figure 3: Schematic view of the continuous flow experimental setup

1.2 Analytical procedure

For ECO of DCF: To check the DCF concentration in EO treated samples, 2 mL sample was withdrawn at fixed time point and quenched with 2 mL methanol (HPLC grade). Sample was immediately mixed in vortex mixer for 30 seconds to ensure complete mixing. The concentration of diclofenac sodium and its intermediates during the electrochemical oxidation was analyzed by high-performance liquid chromatography (HPLC). The HPLC system consisted of liquid chromatography (Shimadzu, LC-2030 Plus) equipped with a C18 column (Shim pack GIST, 250 mm x 46 mm x 5 μ m) and a UV-visible detector. The column temperature was kept at 25 $^{\circ}$ C. The mobile phase contained Acetonitrile (eluent B)/0.1% formic acid (eluent A) = 50/50 at a flow rate of 0.90 mL/min. All solvents were sonicated in an ultrasonic cleaner (make: Labman) for 10 minutes before analysis. The gradient program for this system was: 0.01 to 0.5 min from 50 to 0% Acetonitrile; 0.5 to 6 min from 0 to 100% Acetonitrile; 6 to 9 min from 100 to 0% Acetonitrile; 9 to 10 min from 0 to 50% Acetonitrile; finally returning to the initial conditions. The runtime was 15 min. The injection volume was

100 μ L. UV-vis detector was used to scan absorption at 276 nm wavelength, and the data were analyzed with a LabSolutions software data acquisition system. The iodometric method was used to analyze reactive chlorine species (Palma-Goyes et al., 2016; H. Wang et al., 2019).

For EC/PMS of IBU: To check the IBU concentration in EC/PMS treated samples, a 2 mL sample was withdrawn at the predefined time point. The sample was taken in a test tube containing 2 mL methanol (HPLC grade) to quench reactive species and to stop further IBU degradation. It was mixed instantly using a vortex mixer for 30 seconds to ensure rapid and complete mixing. To avoid iron flocs during IBU analysis in HPLC, samples were centrifuged for 15 minutes. The concentration of IBU during the reaction was analyzed by high-performance liquid chromatography (HPLC). The HPLC system consisted of liquid chromatography (Shimadzu, LC-2030 Plus) equipped with a C18 column (Shim pack GIST, 250 mm x 46 mm x 5 μ m) and a UV-visible detector. The column temperature was kept at 25 $^{\circ}$ C. The mobile phase contained Acetonitrile (eluent B)/0.1% Phosphoric acid (eluent A) = 70/30 at a flow rate of 1.0 mL/min. All solvents were sonicated in an ultrasonic cleaner (make: Labman) for 10 minutes before analysis. UV-vis detector was used to scan absorption at 222 nm wavelength, and the data were analyzed with a LabSolutions software data acquisition system. The runtime was 12 min. The injection volume was 100 μ L. Spectrophotometric methods were used to determine PMS, Fe²⁺, and total Fe concentrations in the samples. For PMS determination in the sample, 1 mL of Titanium (+4) sulfate was added to 2.5 mL of centrifuged sample and mixed for 30 seconds in a vortex mixer. It was then allowed to cool for 10 minutes at room temperature, and solution absorption was measured at 410 nm using a UV-Visible spectrophotometer (Brand: Shimadzu, Model: UV1800, Spectral Bandwidth: 1 nm). Titanium (+4) sulfate was prepared by adding 2.5 g of Titanium dioxide in 250 mL of concentrated sulfuric acid, and this mixture was stirred at 150 rpm and heated at 100 $^{\circ}$ C for 24 h (Rodriguez-Narvaez et al., 2020). For the determination of Fe²⁺ and total Fe, 1,10-phenanthroline method was used (Ling et al., 2017; Tamura et al., 1974). The concentration of Fe³⁺ was calculated by subtracting Fe²⁺ concentration from total Fe concentration.

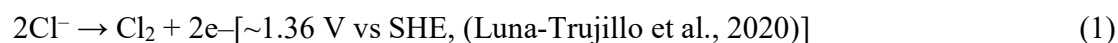
For LC-MS analysis: The system consisted of a Water Acquity UPLC- H Class

equipped with PDA and Acquity SQ detector. Chromatographic separation was performed on Waters X-bridge C18 Column (50*2.1 mm, 2.5 micron); Column temperature: 35 0C, Auto sampler temperature: 15 0C. Chromatographic analysis was carried out using isocratic elution and the mobile phase consisted of Acetonitrile (eluent B) and 0.1% formic acid (eluent A). Mobile phase gradient details are as follows : T = 0 min (97% A, 3% B) flow : 0.8 mL/min; T = 0.75 min (97% A, 3% B) flow : 0.8 mL/min; gradient to T = 2.7 min (2% A, 98% B) flow : 0.8 mL/min; gradient to T = 3 min (0% A, 100% B) flow : 1mL/min; T = 3.5 min (0% A, 100% B) flow : 1 mL/min; gradient to T= 3.51 min (97% A, 3% B) flow : 0.8 mL/min; end of run at T = 4 min (97% A, 3% B). The flow rate was kept 0.8 mL/min, run Time was 4 min, and UV Detection Method was PDA for wavelength range 200 to 500 nm. 10 µL of the samples were injected into the LC system. The analysis was conducted in both the electrospray (ESI) modes: positive and negative. The source working parameters were as follows: cone voltage: 30V and 10 V, capillary voltage: 3.0 KV, extractor voltage: 1 V, rf lens: 0.1 V, temperature of source: 120 °C, temperature of desolvation: 400 °C, cone gas flow: 100 L/hour, desolvation gas flow: 800 L/hour. The MS spectra were recorded in the range of 100 to 1000 m/z.

2. Key Findings

2.1 Electrochemical oxidation of DCF

Electrochemical oxidation of DCF was carried out in RO concentrate which was chloride rich (1.6 g/L). Therefore, the main oxidizing species responsible for degradation would be reactive chlorine species i.e. HOCl, Cl₂, -OCl; and hydroxyl radicals (•OH) (Martínez-Sánchez et al., 2022; Szpyrkowicz et al., 2000, 2007). The contribution of hydroxyl radicals was examined using nitrobenzene as a probe. No significant change was observed in DCF degradation, which means that the contribution of reactive chlorine species was much higher than the contribution of hydroxyl radicals. Moreover, the anode selected in this study - DSA type Ti/Ru-Sn-Sb-Ox MMO- was proven to be active and efficient for in situ electro-generation of RCS species from chlorides (Cruz-Díaz et al., 2018; Feng et al., 2016; García-Espinoza & Nacheva, 2019; Liu et al., 2019). The prevalence of various reactive chlorine species is pH-dependent. RCS arise as HOCl (hypochlorous acid) and/or OCl⁻ (hypochlorous anions) at near-neutral pH, between 5.5 and 7.5. The pH of ROC used in this study ranges from 6.9 to 7.5, which means HOCl and OCl⁻ were predominant species in the degradation of DCF and its IPs (Feng et al., 2016; H. Wang et al., 2019). DCF degradation mechanism can be described as follows: Ti/Ru-Sn-Sb-Ox anode used the electricity supplied in the solution to convert chloride in ROC to chlorine gas (Eq. 1). The chlorine gas reacts with water and HOCl/OCl⁻ are formed at near neutral pH. These reactive chlorine species are responsible for DCF degradation in ROC at near neutral pH. HOCl and OCl⁻ production in an undivided cell can be described by reactions 1, 2, and 3:



Nonetheless, no other reactive chlorine species (i.e. ClO₃⁻, ClO₄⁻) were detected in detectable levels. Also, there are no chances of chlorate (ClO₃⁻) and/or perchlorate (ClO₄⁻)

generation because MMO involved in this study does not have high anodic potential. This is one of the advantages of using MMO over non-active anodes i.e. BDD, PbO₂ while working in a chloride-rich matrix like ROC (Aquino et al., 2012; Barazesh et al., 2016; Feng et al., 2016). To prove the hypothesis that RCS production in large amounts in chloride rich ROC is because of reactions 1, 2, and 3 the concentration of RCS over the time at various current densities is shown in Figure 4.

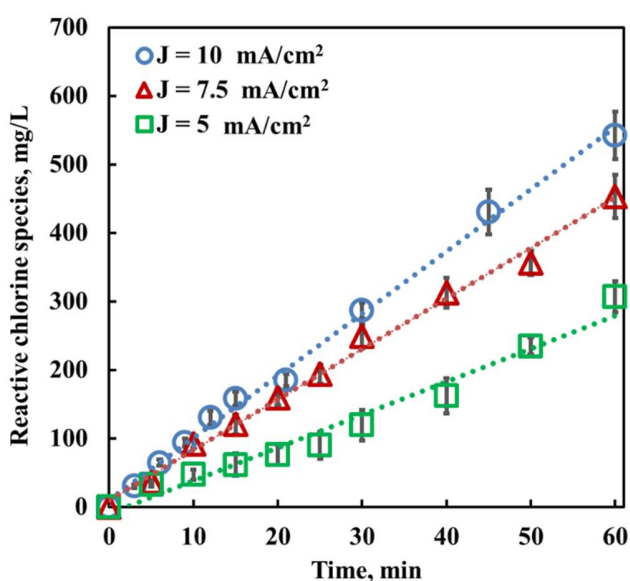


Figure 4: Formation of reactive chlorine species along the time

2.2 Effect of the applied current density and reaction kinetics

Various current densities of values 5, 7.5, and 10 mA/cm² were applied to examine the electrochemical oxidation of DCF and its IPs in ROC. As shown in Figure 5, increase in current density has resulted in faster and complete removal of DCF and its IPs. For lower current density J=5 mA/cm², DCF was not completely removed even after 120 minutes, and IPs were also there. Increasing current density by 2.5 mA/cm² induced faster removal and 98% of DCF and its IPs were removed after 120 minutes when applied current density was 7.5 mA/cm². Further increase in current density by 2.5 mA/cm² showed rapid removal for DCF and especially for IPs. At J = 10 mA/cm² applied density, 99.99% removal was achieved after 120 minutes for both DCF and IPs.

The reason behind this faster removal with increase in current density must be the increasing rate of RCS generation (Liu et al., 2019; Sierra-Rosales et al., 2018). It can be observed by Figure 5 that DCF degradation is quick (in first five minutes), but after the 5th minute time point, for all cases, degradation rate dropped drastically (for 5 min to 120 min). The possible reason for this trend can be explained as follows: HOCl usually causes small changes in the DCF which leads to accumulation of further chlorinated or oxidized DCF. HOCl reactivity is assumed to be higher for DCF in comparison with its reactivity for chlorinated IPs (Barazesh et al., 2016; Deborde & von Gunten, 2008). In addition to this, electrophilic substitution and attacks of HOCl on DCF is normally quick and significant. However, after exhaustion of the substitutable sites, oxidation and addition reactions are ordinarily sluggish (Deborde & von Gunten, 2008).

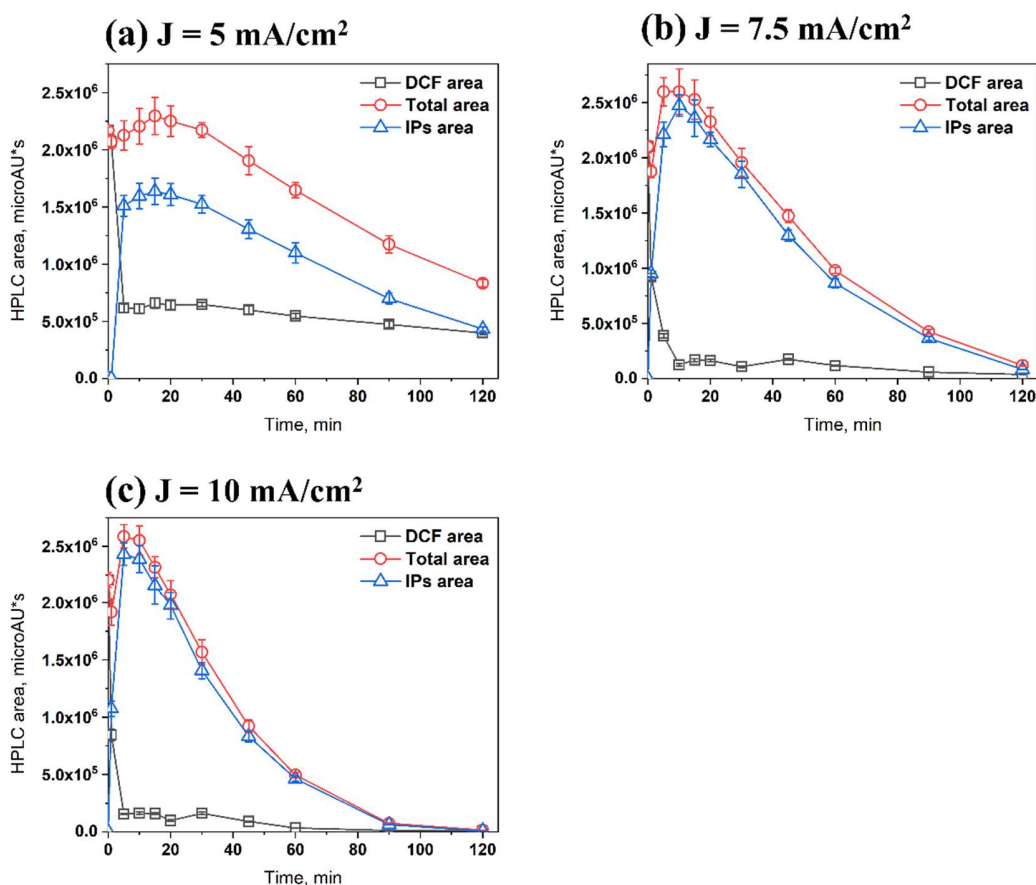


Figure 5: Time course profiles for EO of DCF in ROC, [DCF]₀ = 10 ppm,

**anode: Ti/Ru-Sn-Sb-O_x, cathode: steel, and varying current densities
(a) J=5 mA/cm², (b) J=7.5 mA/cm², and (c) J=10 mA/cm².**

2.3 Effect of electrolyte composition: sulfate to chloride ratio

Electrolyte composition plays an important role in electrochemical oxidation, particularly in indirect electrochemical oxidation which involves diverse reactive chlorine species and/or reactive oxygen species depending upon the electrolyte. Composition of ROC and other real wastewater matrices is dominated by the presence of two main anions, chloride and sulfate ions. The relative concentration of these salts directly affects the formation of reactive species and ultimately the pollutant degradation (Calzadilla et al., 2021; Murrieta et al., 2020; Q. Xiang et al., 2019). To investigate the effect of the relative concentration of these salts on DCF removal, NaCl and Na₂SO₄ salts were added in distilled water to achieve the desired ratio of sulfate ions to chloride ions (S:C). To begin with, five matrices were studied; only chloride, S:C = 0.6 (1.1-0.5), S:C = 1.1, S:C = 1.6 (1.1 + 0.5), and only sulfate. 1.1 was found to be most effective among these five matrices. To fine tune this value, two more ratios were tried, S:C = 0.85 (1.1 - 0.25) and S:C = 1.35 (1.1 + 0.25). These experiments were carried out with 1 L solution at neutral pH and applied current density was 7.5 mA/cm² for 120 minutes.

Figure 6 shows the time course profiles for DCF, IPs, and total (DCF+IPs) area for all seven different matrices. It can be observed that early DCF degradation rate increased with increase in chloride concentration but after a certain point when IPs reached their maximum, further degradation turned out to be extremely slow. On the other hand, DCF degradation rate is 0.6 times lesser for only sulfate matrix than only chloride matrix. If we observe the extent of degradation, only chloride or only sulfate matrices are not at all suitable. When moving from S:C = 0 :1 to S:C = 0.6:1, it can be observed that initial degradation was slower but no significant change was there in total area. Moving ahead, in case of S:C = 0.85 :1, total area was removed noticeably and in case of S:C = 1.1 :1, total area removal was maximum. The ratio S:C = 1.1 :1 was found to be the most effective ratio among all. Forging ahead, increase in sulfate from 1.1 to 1.35 did not show any significant change in removal trend but extent of removal was slightly affected,

total area removal was a little lesser (3%). Increase from 1.35 to 1.6 negatively affected total area removal and degradation rate. In only sulfate medium, there was no removal in total area and DCF was kept slowly transformed to IPs, this matrix showed worst performance among all.

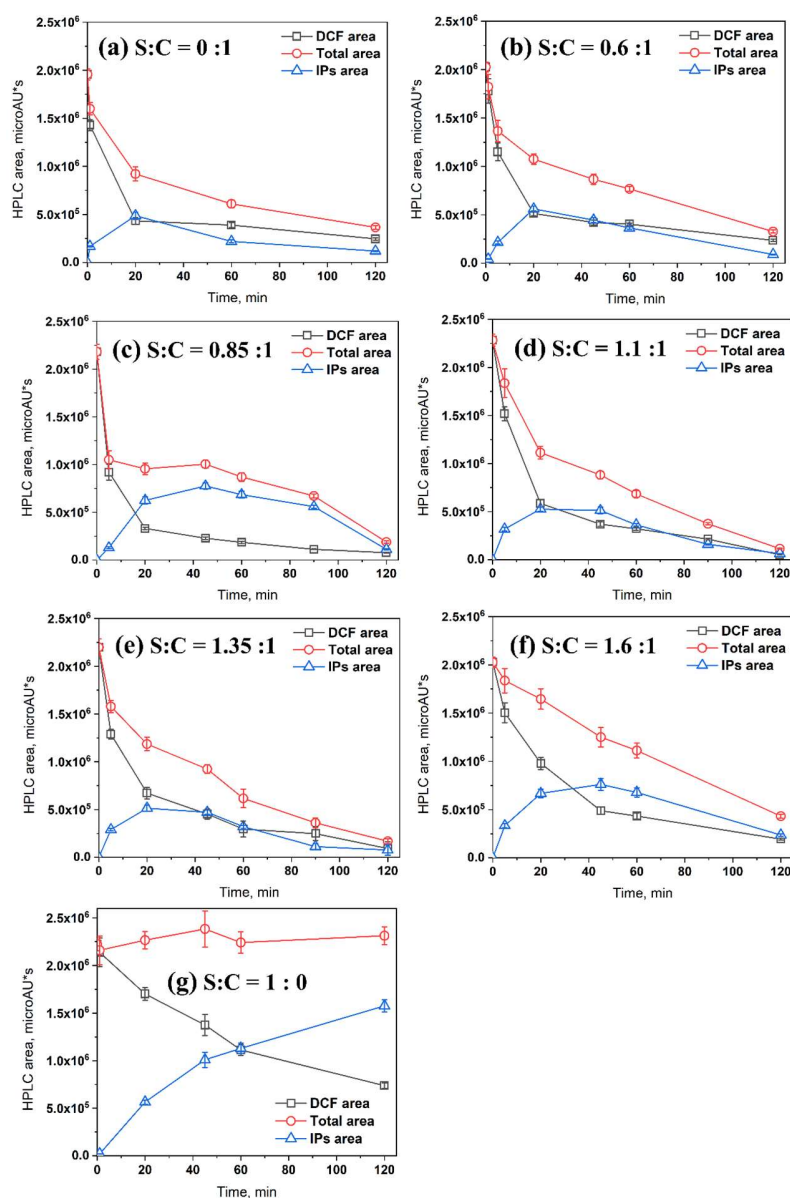


Figure 6: Effect of sulfate to chloride ratio on EO of DCF and its IPs, [DCF]₀ = 10 mg/L, J = 7.5 mA/cm², total salt concentration = 1000 mg/L, anode: Ti/Ru-Sn-Sb-O_x, cathode: steel, (a) [NaCl] = 1000 mg/L and S:C = 0 : 1, (b) [Na₂SO₄]:[NaCl] = 350 : 650 and S:C = 0.6 : 1, (c) [Na₂SO₄]:[NaCl] = 460 : 540 and S:C = 0.84 : 1, (d) [Na₂SO₄]:[NaCl] = 500 : 500 and S:C = 1.1 : 1, (e) [Na₂SO₄]:[NaCl] = 550 : 450 and S:C = 1.35 : 1, (f) [Na₂SO₄]:[NaCl] = 600 : 400 and S:C = 1.6 : 1, (g) [Na₂SO₄] = 1000 mg/L and S:C = 1 : 0.

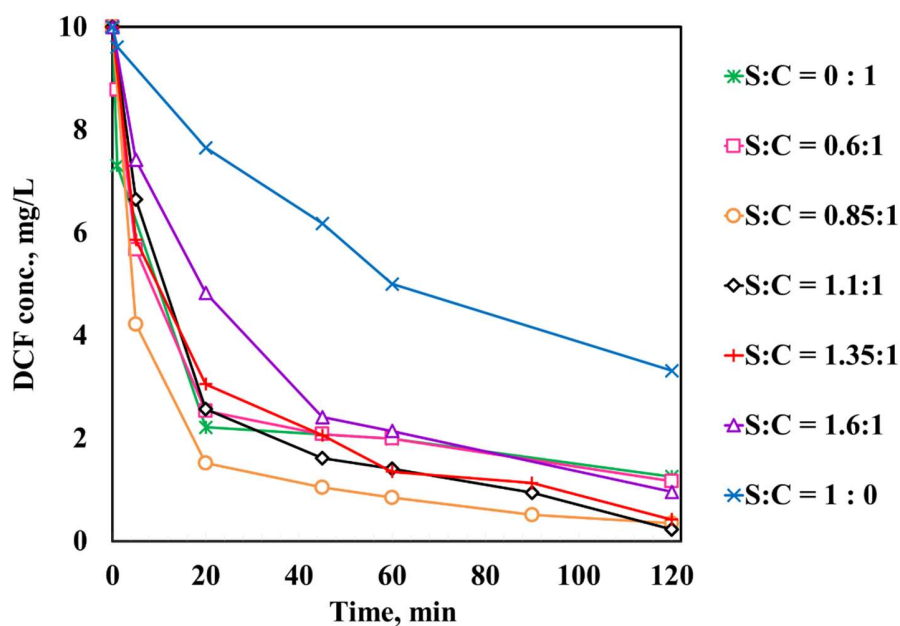


Figure 7: Time course profile for DCF in various S:C composition, $J = 7.5 \text{ mA/cm}^2$, Ti/Ru-Sn-Sb- O_x anode, steel cathode, solution volume = 1 L, $[\text{DCF}]_0 = 10 \text{ mg/L}$

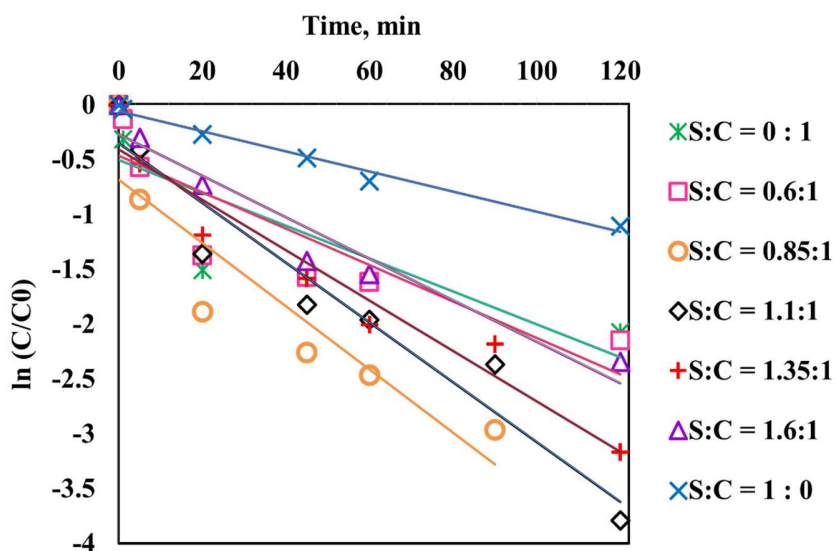


Figure 8: $\ln(C/C_0)$ versus time plot for DCF in various S:C composition, $J = 7.5 \text{ mA/cm}^2$, Ti/Ru-Sn-Sb- O_x anode, steel cathode, solution volume = 1 L, $[\text{DCF}]_0 = 10 \text{ mg/L}$

There are two ways of looking at these results, first is from degradation rate point of view, and second is extent of removal point of view which is total HPLC area removal in this case. Figure 7 shows the time course profiles of DCF and Figure 8 shows $\ln(C/C_0)$ versus time profiles for all S:C ratios. It can be seen from both the figures that sulfate adversely affects the degradation rate of DCF in comparison with chloride, yet it is not always true. If we carefully observe the trend of DCF removal over 120 minutes, reaction rate constant increases from 0.015 min^{-1} to 0.029 min^{-1} for S:C = 0 to 0.85. For S:C >0.85, reaction rate constant started decreasing to -0.019 min^{-1} for 1.6, and it was dropped to 0.009 min^{-1} for only sulfate matrix. This is clearly shown in Figure 8. If we observe the extent of removal, addition of chloride significantly affects the removal (from 1% to 83% for only sulfate to S:C = 1.6 :1 respectively). The extent of removal for all S:C ratios can be assessed from Figure 8. It should be noted that increase in chloride not always helps in total area removal as there is drop from 98% (S:C = 1.1, roughly 48% chloride) to 86% (only chloride, 100% chloride). Hence, it can be concluded that the range $0.85 < \text{S:C} < 1.35$ is the suitable range for DCF degradation and overall extent of removal.

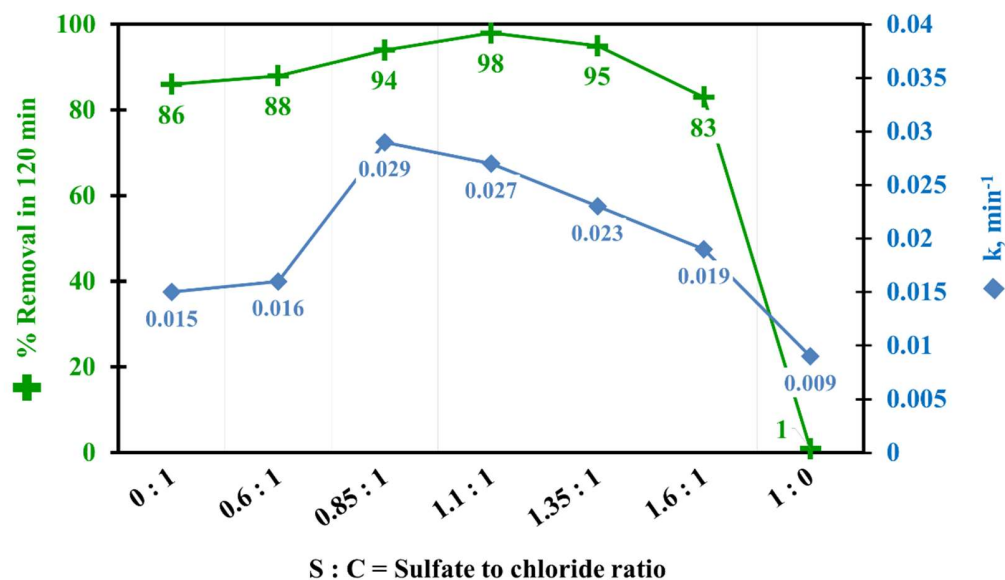


Figure 9: Reaction rate constants for pseudo first order reaction kinetics along with overall (DCF and IPs) % removal for various S:C ratios

It is noteworthy that S:C=1.1 gives maximum removal for DCF and IPs(98%) in synthetic matrix. To further verify this, required amount of sulfate was added in ROC so as to keep S:C = 1.1, and this was used as electrolyte and EO was performed at $J = 7.5 \text{ mA/cm}^2$. The result was totally in agreement with previous experiment done in synthetic matrix. Total removal reached to 99% after sulfate addition. This improvement can be explained from below mentioned reaction:



As per Eq. 5, in presence of sulfate ion, Cl^\bullet reacts with sulfate and this leads to sulfate radical generation to destruct DCF and its IPs (Lan et al., 2017). The composition of electrolyte in terms of sulfate to chloride mass ratio was found to affect the removal of DCF and IPs. The maximum removal (~95%) of DCF was obtained in the presence of sulfate to chloride mass ratio ranging from 0.85 to 1.35. It can be observed from Figure 9 that increase in sulfate concentration (sulfate to chloride mass ratio > 1.35) adversely affect the DCF removal. Overall, the increase in chloride concentration, increases rate and extent of DCF removal. However, at the higher concentration of chloride (sulfate to chloride mass ratio < 0.85), initially higher degradation rate of DCF (0 to 40 min) is significantly retarded (40 to 120 min). It seems that, increased chlorination due to high concentration of chloride ions, may lead to production of highly chlorinated intermediates which resists further degradation.

2.4 Effect of electrode material

Three different electrodes – i. Ti/Ru-Sn-Sb- O_x , ii. Ti/Ru-Ir- O_x , and iii. Graphite were used as an anode keeping other reaction parameters same, to evaluate the effect of electrode materials. It can be seen from the Figure 10a, that initially (within five minutes) degradation rate was faster for Ti/Ru-Sn-Sb- O_x , in comparison with other two electrodes. But as the time progressed, DCF degradation was sluggish in case of Ti/Ru-Sn-Sb- O_x . Similarly, in case of Ti/Ru-Ir- O_x , DCF degradation continued for first ten minutes, then degradation remarkably slowed down. However, in case of Graphite, degradation continued till one hour at slower rate, but degradation extent was maximum in this case. DCF was completely removed in two hours but the IPs were maximum in case of ECO using Graphite (Figure 10b). It can be observed from Figure 10b that intermediates

were minimum for ECO using Ti/Ru-Sn-Sb-O_x, at the end of two hours. When experiment was carried out at higher densities $J = 7.5$ and 10 mA/cm^2 , graphite plate was started corroding and carbon particles were appearing in solution. Nonetheless, for Ti/Ru-Sn-Sb-O_x and Ti/Ru-Ir-O_x, when higher current densities were applied, degradation rate and extent both were improved. The DCF and its IPs were completely removed when applied current density was 7.5 mA/cm^2 . Therefore, Ti/Ru-Sn-Sb-O_x was used as an anode for other experiments. The enhanced removal of DCF and its intermediates could be due to electro-catalytic activity of Ru, Sn, and Sb oxides coating (Cruz-Díaz et al., 2018; Martínez-Sánchez et al., 2022). Three different electrodes – i. Ti/Ru-Sn-Sb-O_x, ii. Ti/Ru-Ir-O_x, and iii. Graphite were used to evaluate the effect of electrode materials. It can be seen from the Figure 10, that initially degradation rate was faster for Ti/Ru-Sn-Sb-O_x, in comparison with other two electrodes. But as the time progressed, DCF degradation was sluggish in case of Ti/Ru-Sn-Sb-O_x. Therefore, developing novel low-cost electrodes, such as the fusion of transition metals along with noble metals, can impart enhanced electro-catalytic activity and simultaneously reduce the cost of the catalysts.

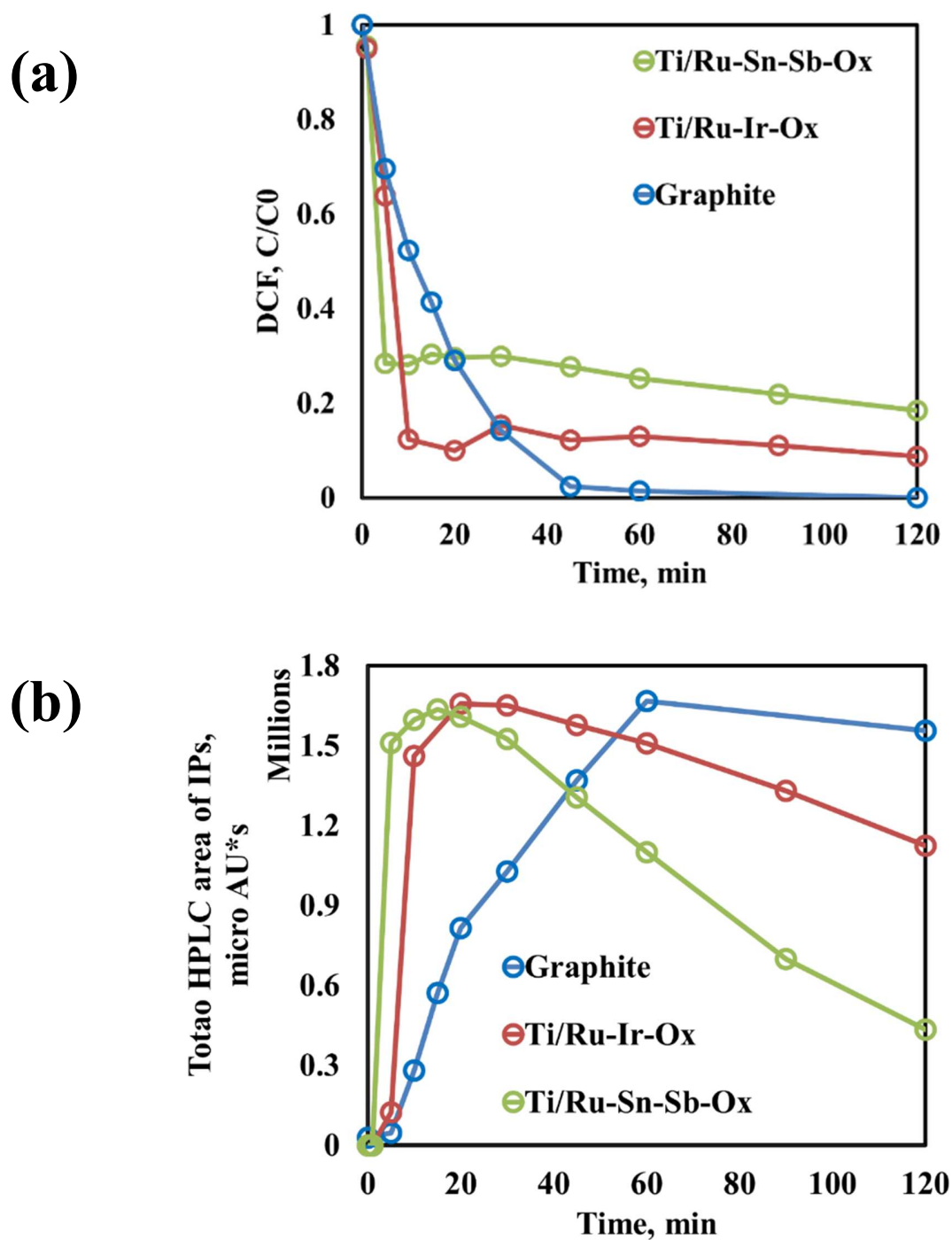


Figure 10: Time course profiles for DCF and its IPs using ECO with three different electrodes, matrix = ROC, $J = 5 \text{ mA/cm}^2$, steel cathode, solution volume = 1 L, $[\text{DCF}]_0 = 10 \text{ mg/L}$, $\text{pH} = 7.8$

2.5 Phytotoxicity study

The treatment can be said to be efficient only when high removal efficiency is achieved along with the effluent which is safe to be discharged in environment. To avoid any harm to plants when the treated solution would be applied for irrigation purpose, carrying out phytotoxicity test is necessary. In this study, Mung bean seeds were used for phyto-toxicological analysis of ROC spiked with 10 mg/L DCF, before and after electrochemical oxidation. The results for the study are tabulated in Table 2. Germination % and average radicle length are two crucial parameters in development of plant and also are sensitive towards pollutants (Stupar et al., 2020). Generally, distilled water is taken as control for calculating the phytotoxicity % because most experiments are carried out in synthesized wastewater prepared from distilled water. In this study, distilled water was taken as a check only and ROC was selected as control because ROC was spiked with DCF for EO experiments. Reaction conditions for final sample taken in consideration were: $J = 7.5 \text{ mA/cm}^2$, ROC, $[\text{DCF}]_0 = 10 \text{ mg/L}$, Ti/Ru-Sn-Sb- O_x anode steel cathode, $\text{pH} = 7.5 \pm 0.2$, and 120 minutes electrolysis time. It can be noted that germination was not significantly affected in comparison with a previously reported study for dye removal using EO which showed 72% after 1780 min of treatment (Mijin et al., 2012). Similarly for phytotoxicity, initial value was 3% which is negligible, and it was elevated to 9% after 120 min of treatment. Though there was an increment, yet it was not substantial enough to cause any harm if reused for irrigation purpose (Santos et al., 2020; Vijayakumar et al., 2021). However, such reuse application must be carried out after thorough analysis of other water quality parameters. Furthermore, to ensure that there is no uptake of any trace DCF or IP in mung beans, retentate was analyzed in HPLC and there was no significant change in HPLC peaks. Figure 11 shows graphical representation of the results for phytotoxicity test.

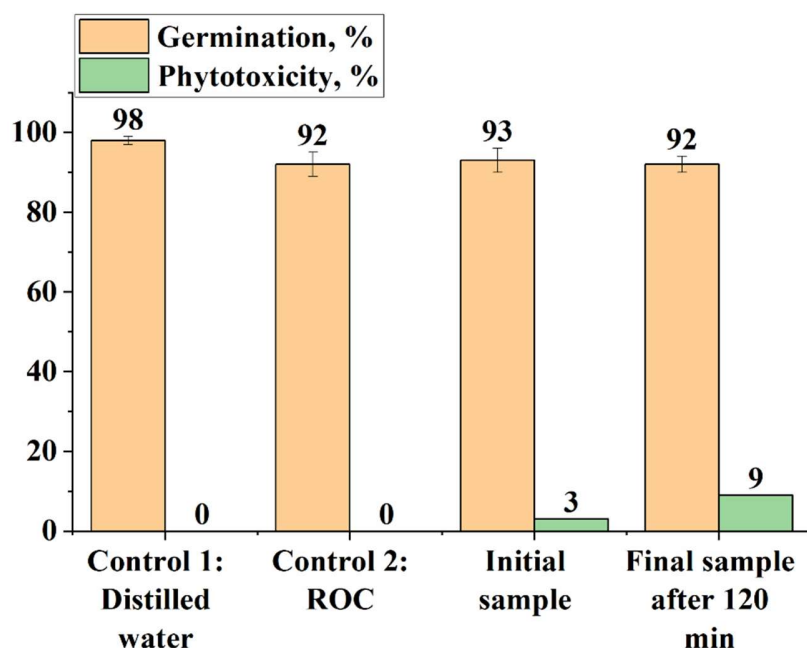


Figure 11: %Germination and %Phytotoxicity for mung seeds in distilled water, ROC, initial sample (ROC spiked with 10 mg/L DCF), and treated sample by EO for 120 minutes

2.6 Comparative study of EC alone, PMS alone, EC/PMS, and $\text{Fe}_2\text{SO}_4/\text{PMS}$

IBU removal was first observed for five different processes: (a) Electrolysis using iron as an anode (EC alone), (b) PMS alone, (c) Electrochemically activated peroxymonosulfate using iron as anode (EC/PMS process), (d) PMS activation by Fe^{2+} using ferrous sulfate heptahydrate where an equivalent amount of ferrous ($[\text{Fe}^{2+}]_0 = 99.12 \text{ mg}$) was added at the initial point ($t=0$), and (e) PMS activation by Fe^{2+} where one sixth of an equivalent amount of ferrous ($[\text{Fe}^{2+}]_0 = 16.52 \text{ mg}$) was added in six steps, eventually total Fe^{2+} added in 30 min would be 99.12 mg (16.52 mg Fe^{2+} was added at $t=0, 5, 10, 15, 20, 25 \text{ min}$; 6 time points).

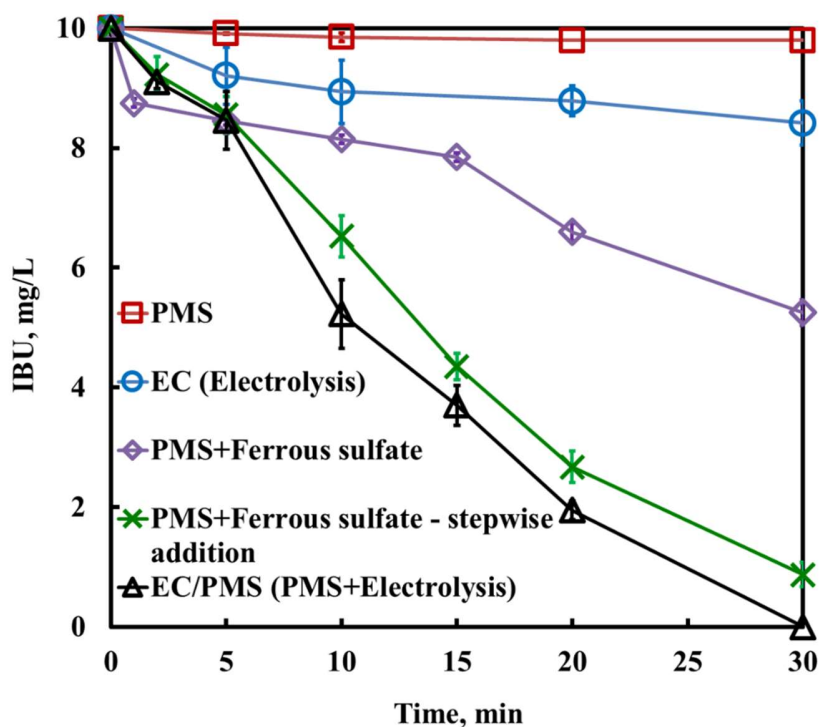
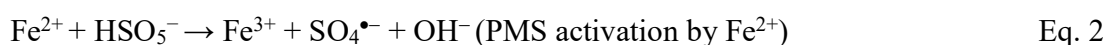
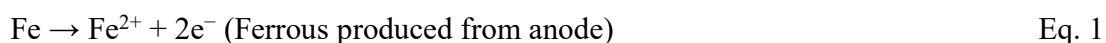


Figure 12: IBU removal in ROC matrix under different systems. Experimental conditions: $[IBU]_0 = 10 \text{ mg/L}$, $[PMS]_0 = 500 \text{ mg/L}$, total $[Fe^{2+}] = 99.12 \text{ mg/L}$, current density = 2.5 mA/cm^2 , $pH_0 = 7.5$

As shown in Figure 12, when IBU was degraded by PMS alone in ROC, only 2 % removal in 30 min was observed because PMS has limited oxidation ability (redox potential $E_0 = 1.82 \text{ V}$) at room temperature and neutral pH (Bu et al., 2017; Qiong et al., 2021). Electrolysis using iron electrode (which can also be considered as electrocoagulation) achieved 18 % IBU removal in 30 minutes, it can be inferred that the coagulation mechanism contributed to IBU removal. Surprisingly, electrochemically activated peroxymonosulfate using iron as anode and graphite as the cathode (EC/PMS process) achieved complete removal in 30 minutes. In EC/PMS process, ferrous was generated electrochemically from the sacrificial iron anode (Eq. 1), which is responsible for PMS activation and leads to sulfate radical ($SO_4^{\bullet-}$) production (Eq. 2) (Qiong et al., 2021; Y. R. Wang & Chu, 2011). Sulfate radical attacks the IBU compound and quicken the IBU removal (Eq. 3). Besides this, PMS is also activated by electron gain and produce sulfate radical (Eq. 4) and hydroxyl radical (Eq. 5) that further supports IBU oxidation (Yang et al., 2015).

PMS gets activated through Fe^{3+} as well (Eq. 6) and produce peroxymonosulfate radical which is weaker than sulfate radical. In addition to that, chloride present in ROC reacts with PMS which leads to HOCl formation, which also attacked the IBU (Eq. 7) (Govindan et al., 2014; Y. R. Wang & Chu, 2011). Furthermore, there is possibility of Fe^{2+} regeneration on graphite cathode (Eq. 8) and this might enhance the IBU removal (Qiong et al., 2021). To verify the contribution of cathode and also the logic that iron anode is merely used to supply Fe^{2+} or direct oxidation occurred at the anode surface, PMS activation process was carried out using ferrous sulfate heptahydrate. According to Faraday's law ($C = (I*t)/(F*Z*V)$), for 30 min reaction with 2.5 mA/cm² current density (190 mA current) gives 99.12 mg Fe^{2+} . 99.12 mg Fe^{2+} was added in two ways, (i) total 99.12 mg Fe^{2+} was added at initial time point $t=0$, and (ii) 16.52 mg Fe^{2+} was added at $t=0$ and then 16.52 mg Fe^{2+} was added stepwise at every 5 minutes ($t = 5, 10, 15, 20, 25$ min) so that total 99.12 (16.52*6) mg Fe^{2+} was added in total 30 min. It is interesting to note that when total ferrous was added at start, removal was faster in first five minutes, but after that removal was slowed down and 46% removal was achieved in 30 min; whereas, when ferrous was added stepwise, it showed consistent removal throughout and 90% removal was achieved in 30 min (Figure 12). It implies that excess of ferrous at initial point quicken the removal in first five minutes cause of more sulfate radical formation than EC/PMS process, but relatively high concentration of ferrous quenched sulfate radicals and slowed down the removal (Bu et al., 2017; Du et al., 2019). On the other hand, stepwise addition gave similar performance to that of EC/PMS process cause in EC/PMS also Fe^{2+} generation is gradual; the only difference is, in former process Fe^{2+} was added manually and in later process it was generated electrochemically (Figure 12 & Figure 13). Though 10% more IBU removal in case of EC/PMS process could be attributed to Fe^{2+} regeneration from Fe^{3+} on cathode. As illustrated in Figure 13, EC/PMS and PMS activation by ferrous sulfate followed pseudo first order reaction kinetics. The apparent removal rate constants follow the order of EC/PMS (0.073 min^{-1}) > Fe^{2+} stepwise addition/PMS (0.071 min^{-1}) > Fe^{2+} /PMS (0.021 min^{-1}) > EC (0.0065 min^{-1}) > PMS (0.0008 min^{-1}).



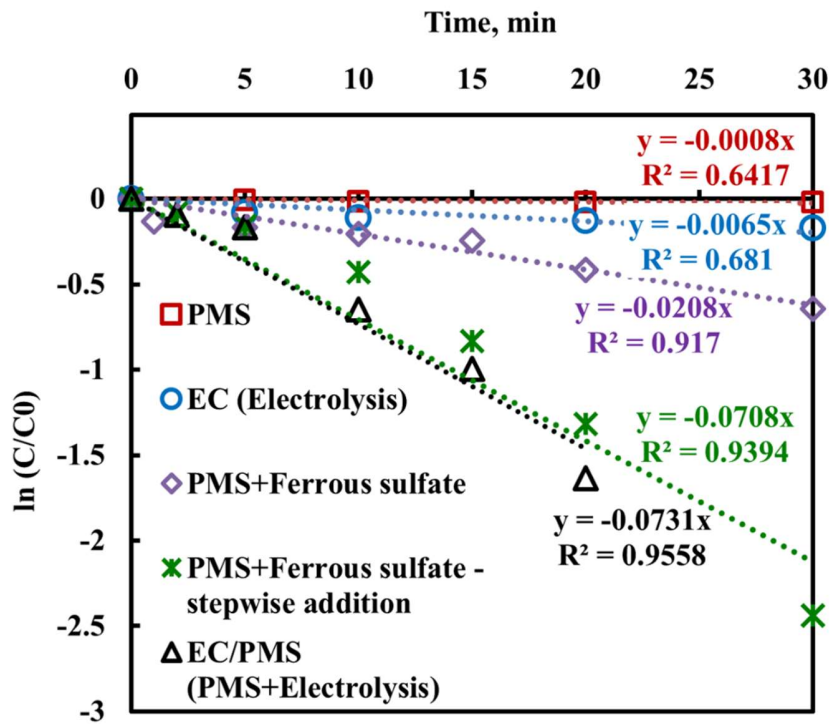
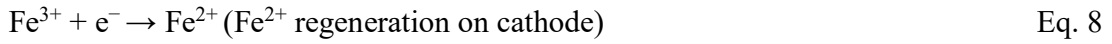
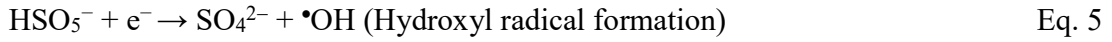
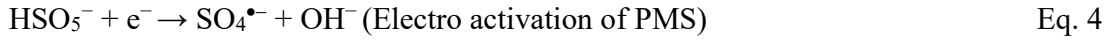


Figure 13: Comparison of different systems on the basis of reaction rate. Experimental conditions: $[\text{IBU}]_0 = 10 \text{ mg/L}$, $[\text{PMS}]_0 = 500 \text{ mg/L}$, $[\text{Fe}^{2+}] = 99 \text{ mg/L}$, current density = 2.5 mA/cm^2 , $\text{pH}_0 = 7.5$

2.7 Results of response surface methodology

3D response surfaces and contour plots: Figures 14, 15, and 16 show the 3D response surfaces and their matching contour plots of IBU removal rate constants over PMS conc. and CD, pH and CD, and pH and PMS conc. respectively based on developed 2FI model. Figure 14 shows the effect of pH for given PMS conc. and CD on IBU removal rate constant. It can be observed that the acidic pH 5.5 is the most favourable for EC/PMS process with 100 mg/L PMS and 4.475 mA/cm² CD, where removal rate constant increased beyond 0.275 min⁻¹. As pH increased to 7.5, removal rate decreased to 0.2 min⁻¹ for the same values of PMS and CD whereas alkaline pH 9.5 is not at all suitable for the EC/PMS process cause removal rate constant dropped below 0.125 min⁻¹. As shown in Figure 14a, for pH 5.5, removal rate constant decreased with increasing PMS conc. and decreasing CD. The availability of Fe²⁺ for PMS activation is highly dependent on pH. In alkaline pH, ferrous or ferric ions get converted to iron hydroxides and it leads to decrease in Fe²⁺ availability and the reduction of radical generation and ultimately slowing down the IBU removal. Figure 15 shows the effect of PMS concentration for given values of pH and CD. It is interesting to note that lower PMS conc. 100 mg/L is optimum for maximum IBU removal rate constant and rate constant decreased with increasing PMS concentration for similar combinations of pH and CD. For [PMS]₀=100 mg/L, as shown in Figure 15a, removal rate constant decreased with increase in pH and decreased CD. The reason behind this could probably be quenching of sulfate radical and hydroxyl radical by excess PMS at the start of PMS activation (Qiong et al., 2021). Figure 16 shows the effect of CD for given values of pH and PMS conc. It is quite obvious that increase in CD enhances the IBU removal, as the Fe²⁺ generation increases which activates the PMS. For initial pH=5.5 and PMS=100 mg/L, removal rate constant is highest - above 0.275 min⁻¹ for higher CD 4.475 mA/cm². As CD decreased to 2.5 mA/cm², removal rate constant decreased to 0.2 min⁻¹; and further decrease in CD to 0.525 mA/cm² resulted in dropping of removal rate constant below 0.125 min⁻¹. It can be concluded from Figures 14, 15, and 16 that acidic pH, lowest initial PMS conc., and highest current density were promoting the rate constants for IBU removal using EC/PMS process.

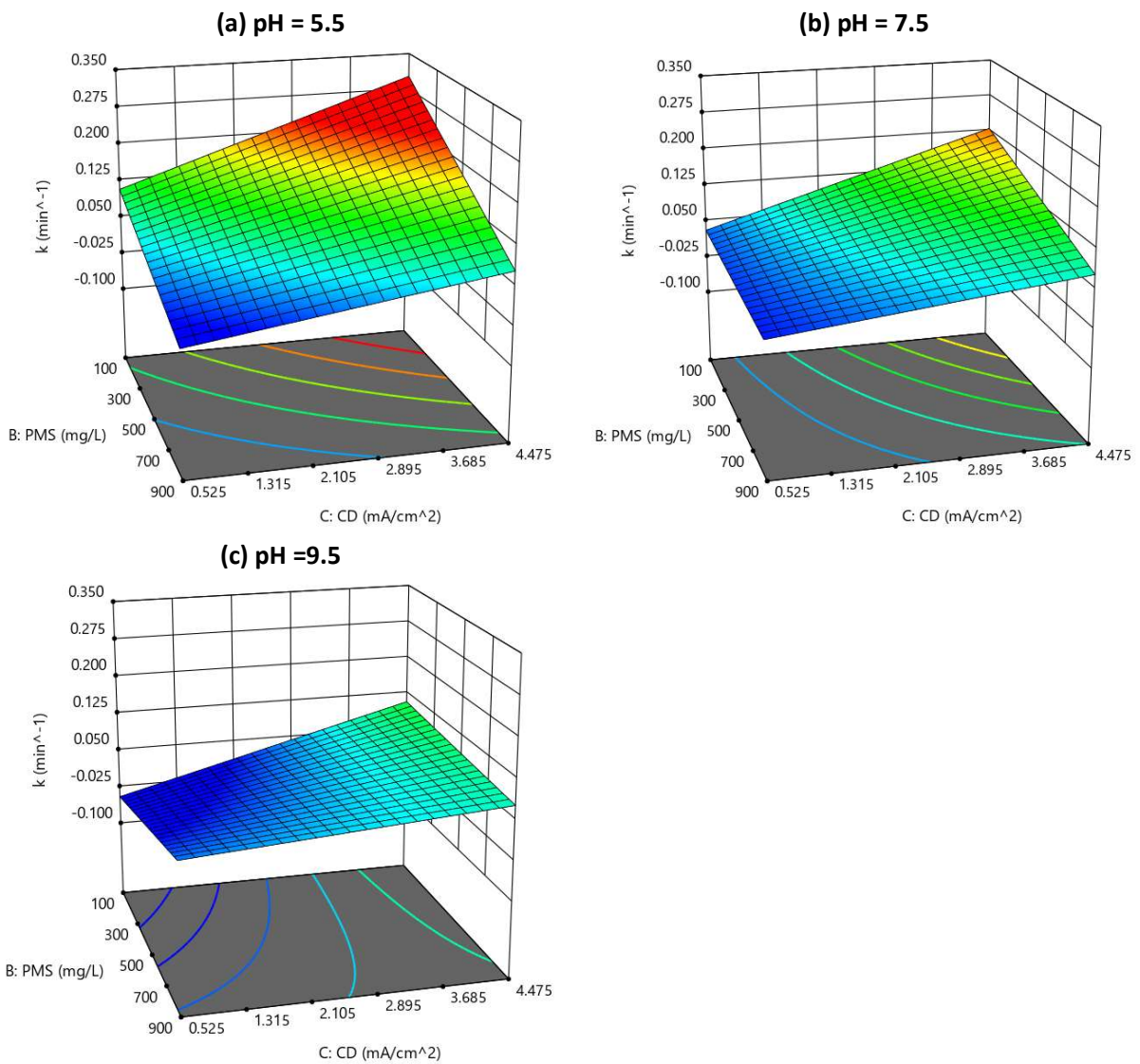


Figure 14: Effect of pH on IBU removal rate constant for various combinations of current densities and $[PMS]_0$. Experimental conditions: ROC, $[IBU]_0 = 10$ mg/L.

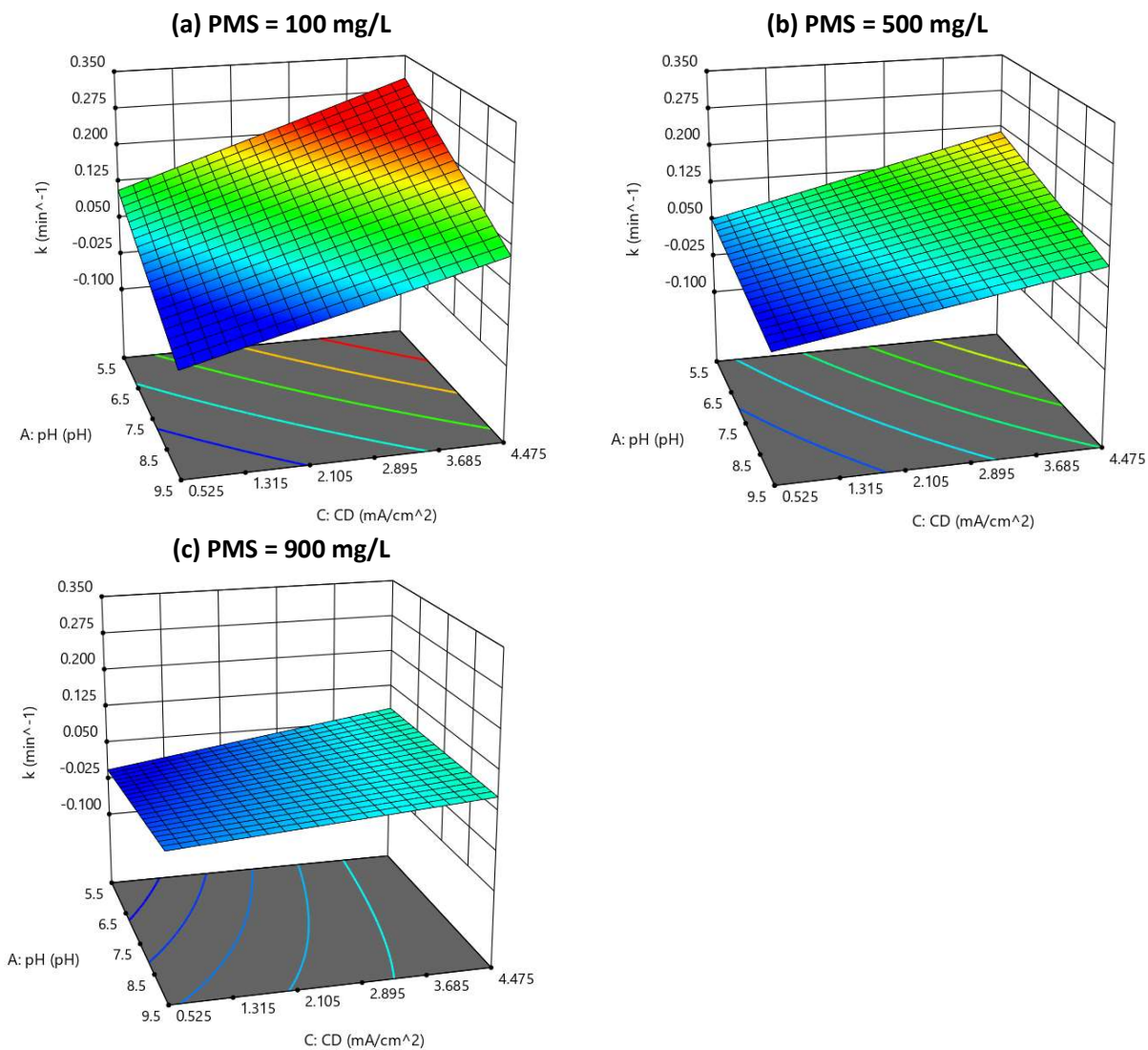


Figure 15: Effect of initial PMS concentration on IBU removal rate constant for various combinations of pH and current densities. Experimental conditions: ROC, $[IBU]_0 = 10 \text{ mg/L}$.

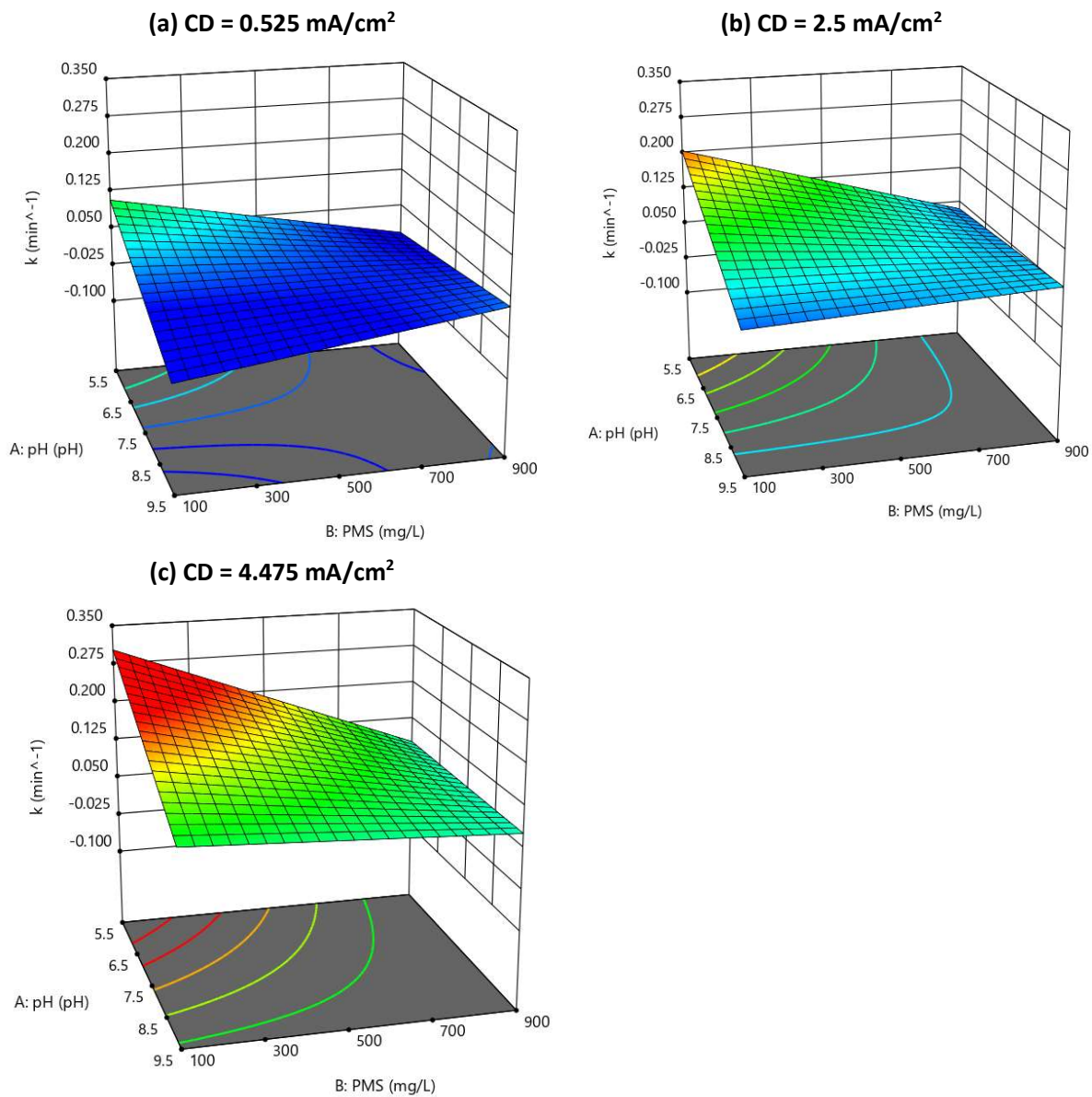
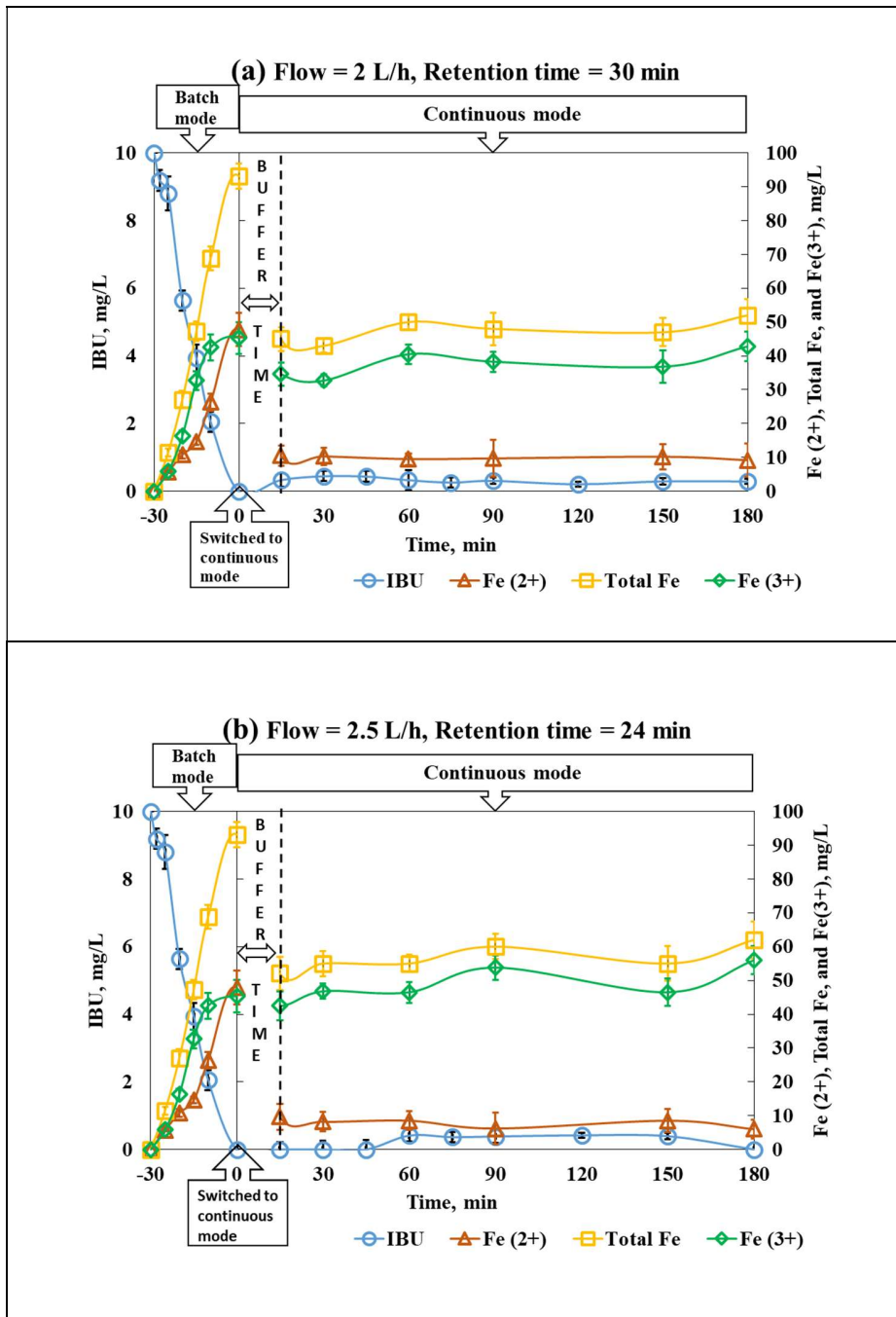


Figure 16: Effect of current density on IBU removal rate constant for various combinations of pH and $[PMS]_0$. Experimental conditions: ROC, $[IBU]_0 = 10 \text{ mg/L}$.

2.8 Performance in continuous flow mode

As discussed in previous section, 7.5 initial pH, 500 mg/L $[PMS]_0$, and 2.5 mA/cm² achieved complete IBU removal using EC/PMS process. Thus this combination was selected for continuous flow experiments. Reactor was initially operated in batch mode for 30 minutes and then fresh solution containing 10 mg/L IBU and 500 mg/L $[PMS]_0$ was introduced in the reactor. The flow was kept 2 L/h for the preliminary experiment and samples were withdrawn after 15 minutes from the switch to continuous mode. As shown in Figure 17a, IBU conc. in the outlet of continuous flow reactor was ranging from 0.2 to 0.5 mg/L (average 0.35 mg/L, 96.8% removal) and average values of Fe²⁺, Fe³⁺, and total Fe conc. were 9.9, 37.6, and 47.5 mg/L respectively. It is noteworthy that while in batch mode (-30 to 0 min), 500 mg/L PMS was added at the start and from that point to next 30 min, PMS was consumed and Fe²⁺ and Fe³⁺ was generated continuously. As the feed started, PMS was introduced again with IBU and Fe²⁺ was further consumed in PMS activation which led to decrease in Fe²⁺ conc. and also Fe³⁺ conc. The molar ratio of IBU: Fe²⁺: PMS was 1: 37.5: 68.5, for 2 L/h flow and 30 min residence time. To achieve the complete IBU removal and maximum consumption of Fe²⁺ in PMS activation (maximum current efficiency), flow rates were increased to 2.5, 3, and 4 L/h giving residence time (RT) 24, 20, and 15 min respectively (Kobya et al., 2016; Sravanth et al., 2020). As illustrated in Figure 17b, 17c, and 17d, increased flow attained more % IBU removal and lesser residual Fe²⁺ appeared in outlet. For 2.5, 3, and 4 L/h flow, IBU: Fe²⁺: PMS molar ratios were 1: 30: 68.5, 1: 25: 68.5, and 1: 19: 68 respectively and average % IBU removal were 97.8%, 98.7%, and 99.5% respectively. Here also, there is strong correlation between PMS to Fe²⁺ ratio and % IBU removal. As PMS to Fe²⁺ ratio increased from 1.8 to 3.6, average % IBU removal increased from 96.5% to 99.5%.



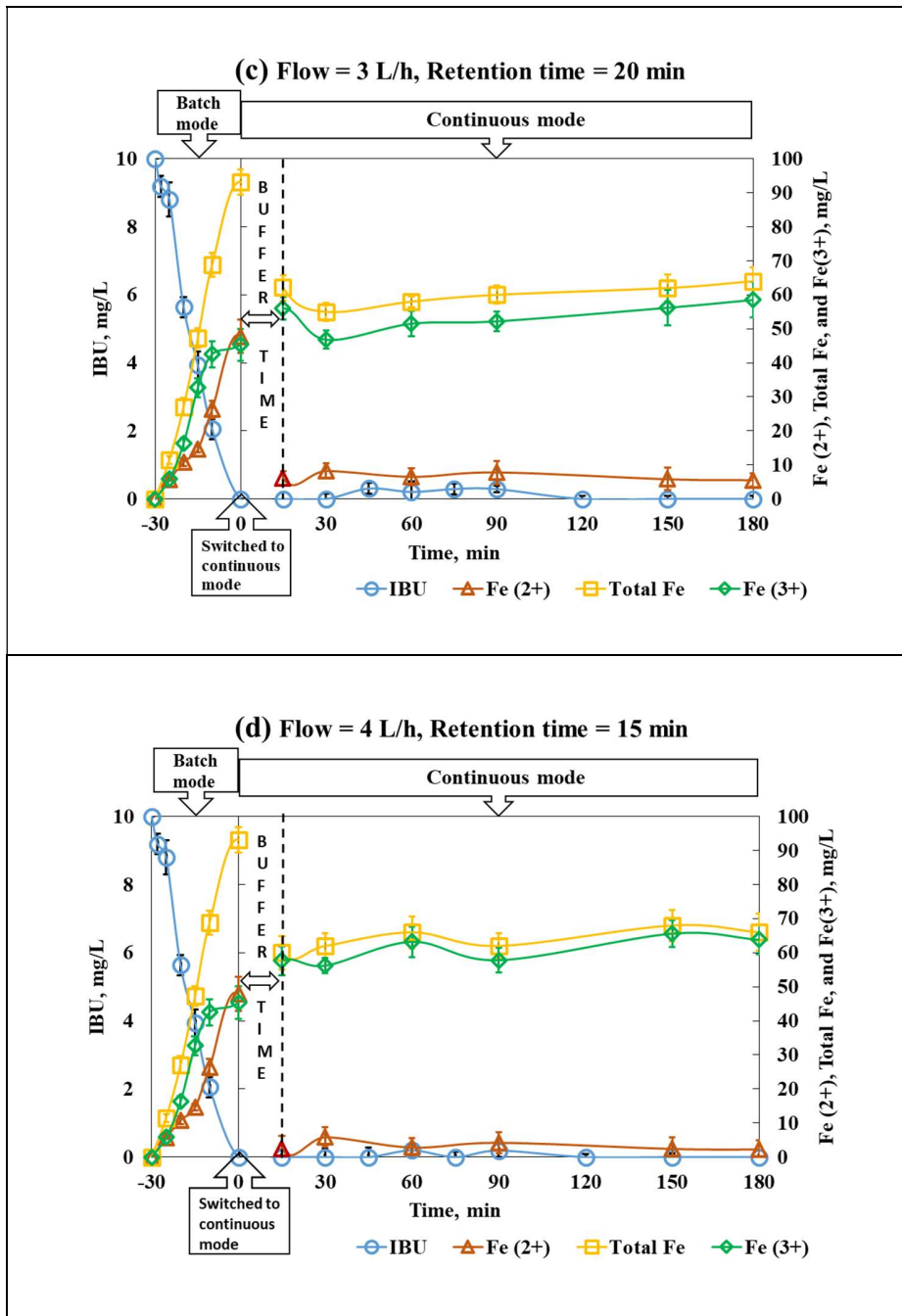


Figure 17: Effect of flow (residence time - RT) on the performance of continuous EC/PMS process (a) Flow = 2 L/h, RT = 30 min, (b) Flow = 2.5 L/h, RT = 24 min, (c) Flow = 3 L/h, RT = 20 min, (d) Flow = 4 L/h, RT = 15 min.

2.9 Results of LC-MS analysis

LC-MS analysis was carried out to identify the intermediates formed while ECO of DCF and EC/PMS of IBU in ROC.

As depicted earlier, during ECO of DCF, two intermediates were formed at RT 8.5 min and 9.1 min. To identify the molecular mass and structure of these compounds, LC-MS analysis was carried out. As shown in Figure 18, mass of DCF was confirmed as m/z 296. Mass of IP_{8.5} was found to be m/z 310.2 and mass of IP_{9.1} was found to be m/z 314.1. According to the fragmentation pattern and published reports, the hydroxylation products of DCF from indirect oxidation were proposed as shown in the Figure 18.

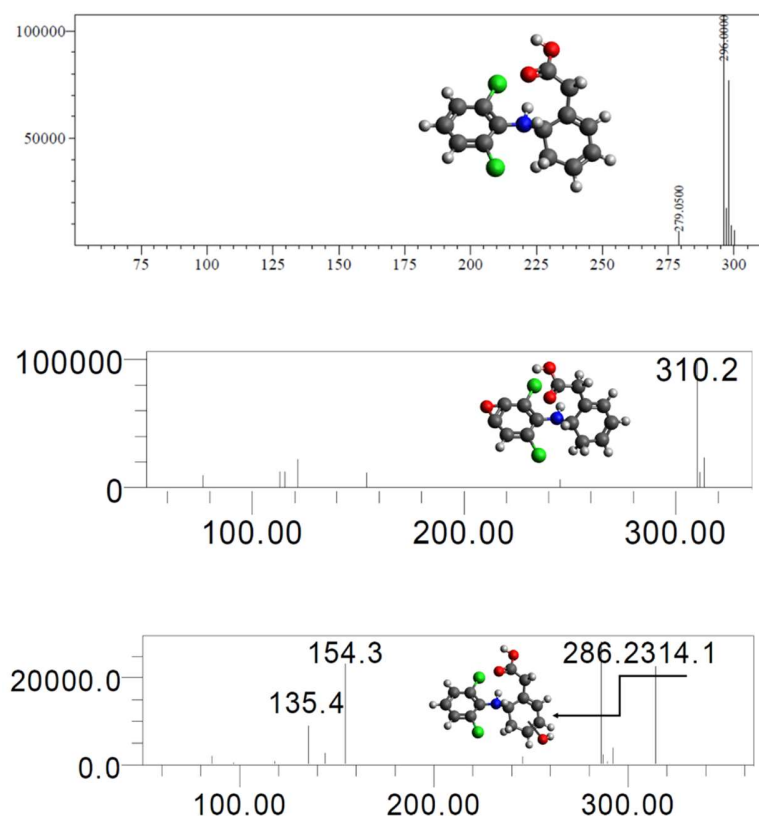


Figure 18: LC-MS spectra of DCF (m/z 296), IP_{8.5} (m/z 310), and IP_{9.1} (m/z 314). (Colour coding: Black=Carbon, Grey=Hydrogen, Red=Oxygen, Green=Chlorine, Blue=Nitrogen).

Similarly, the intermediate was observed in HPLC chromatograms of samples containing IBU after EC/PMS process. IBU appeared at 222 nm and when sample was scanned at 260 nm, the intermediate was increasing with the decrease in IBU conc. Therefore, LC-MS analysis was carried out to identify the mass and structure of the intermediate appearing at 260 nm (refer Appendix K). As depicted in Figure 19, IBU was confirmed at 222 nm with m/z 206.3, and m/z of the intermediate was found to be 238. Quite similar to the ECO of DCF, here also, hydroxylation product of IBU was proposed as suggested by published literature and fragmentation pattern. Brillas, 2022 and Y. Xiang et al., 2016 also reported this oxidation product of IBU using UV/chlorination and Catalytic Ozonation/PMS respectively.

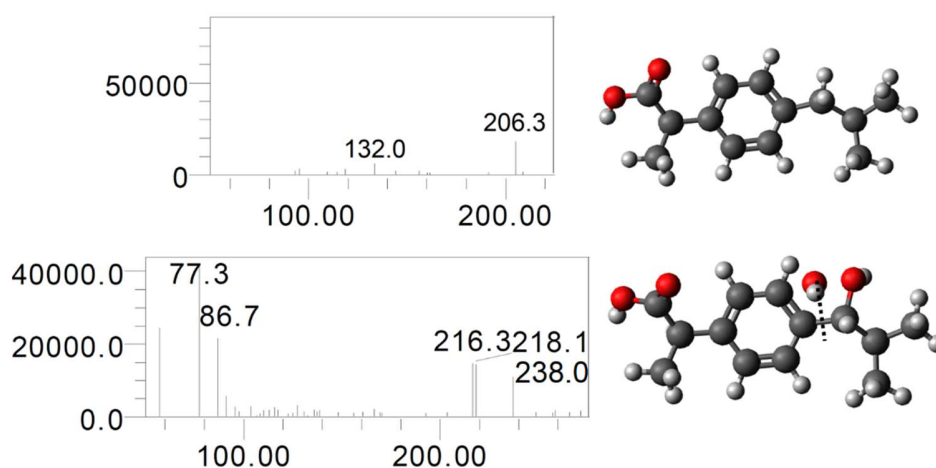


Figure 19: LC-MS spectrums of IBU (m/z 206.3) and IP@_{260 nm} (m/z 238). (Colour coding: Black=Carbon, Grey=Hydrogen, Red=Oxygen, Green=Chlorine, Blue=Nitrogen).

3. Conclusion

From the results discussed so far, following conclusions can be made:

- Among various agents/techniques, methanol quenching and refrigeration showed better correlation ($R^2 \geq 0.99$) and nitrite showed reasonable correlation ($R^2 = 0.94$). The p value 0.005 obtained using paired t-test indicated that the results obtained using methanol as quenching agent matches with those obtained by immediate analyses (without quenching) with 99.5% confidence level. Thus, methanol is the most suitable quenching agent in the present study.
- The removal rate increased with increase in current density from 5 to 10 mA/cm² for DCF and IPs both. For $J = 7.5$ and 10 mA/cm², DCF and both intermediates were removed in 120 min.
- The composition of electrolyte in terms of sulfate to chloride mass ratio was found to affect the removal of DCF and IPs. The maximum removal (~95%) of DCF was obtained in the presence of sulfate to chloride mass ratio ranging from 0.85 to 1.35. An increase in sulfate concentration (sulfate to chloride mass ratio > 1.35) adversely affect the DCF removal. Overall, the increase in chloride concentration, increases rate and extent of DCF removal. However, at the higher concentration of chloride (sulfate to chloride mass ratio < 0.85), initially higher degradation rate of DCF (0 to 40 min) is significantly retarded (40 to 120 min).
- In comparison with Graphite anode, MMO coated anodes Ti/Ru-Sn-Sb-O_x and Ti/Ru-Ir-O_x were found to be efficient for DCF and IPs removal. DCF degradation rate was fastest while using indigenously prepared MMO Ti/Ru-Sn-Sb-O_x.
- Keeping ROC as control, increment in phytotoxicity level was 6% after 120 min of EO which is not significant enough as compared with similar previous studies. Hence, it was presumed that the treated solution could be reused for irrigation purpose.
- EC/PMS process attained complete IBU removal in 30 min and performed better than PMS activation using chemical sources for Fe²⁺ in ROC matrix.
- Quenching experiments using TBA and ethanol indicated that the contribution of sulfate radical is quite higher than hydroxyl radical for IBU removal in ROC using EC/PMS process.

- RSM was performed to understand the effect of pH, $[PMS]_0$, and CD on the % IBU removal in 30 min and removal rate constants as long as the reaction follow pseudo first order. It was observed that acidic pH=5.5, lesser $[PMS]_0=100$ mg/L, and highest CD=4.475 mA/cm² is favourable for higher removal rate constants. However, higher removal rate constant does not necessarily lead to complete removal. Complete removal was achieved in near neutral pH=7.5, at $[PMS]_0=500$ mg/L, and CD=2.5 mA/cm². At pH=7.5, increase in $[PMS]_0$ beyond 500 mg/L and CD beyond 2.5 mA/cm² did not attain faster removal.
- $[PMS]_0$ to CD ratios significantly affect both %IBU removal and removal rate constant in batch EC/PMS process. Mostly, lower ratios achieved greater removal rate constants and % IBU removal. For $[PMS]_0$ to CD ratio = 200, % IBU removal was >95% for all pH.
- EC/PMS process functioned quite well in continuous flow mode. The increase in flow rate from 2 to 4 L/h gave higher % IBU removal 96.5% to 99.5% and residual Fe²⁺ was reduced from 10 to 3 mg/L respectively.
- LC-MS results showed that DCF and IBU intermediates were hydroxylation products of indirect oxidation.

References

- Aquino, J. M., Rodrigo, M. A., Rocha-Filho, R. C., Sáez, C., & Cañizares, P. (2012). Influence of the supporting electrolyte on the electrolyses of dyes with conductive-diamond anodes. *Chemical Engineering Journal*, 184, 221–227. <https://doi.org/10.1016/j.cej.2012.01.044>
- Barazesh, J. M., Prasse, C., & Sedlak, D. L. (2016). Electrochemical Transformation of Trace Organic Contaminants in the Presence of Halide and Carbonate Ions. *Environmental Science and Technology*, 50(18), 10143–10152. <https://doi.org/10.1021/acs.est.6b02232>
- Brillas, E. (2022). Chemosphere A critical review on ibuprofen removal from synthetic waters , natural waters , and real wastewaters by advanced oxidation processes. *Chemosphere*, 286(P3), 131849. <https://doi.org/10.1016/j.chemosphere.2021.131849>
- Bu, L., Zhou, S., Shi, Z., Bi, C., Zhu, S., & Gao, N. (2017). Iron Electrode as Efficient Persulfate Activator for Oxcarbazepine Degradation : Performance , Mechanism , and Kinetic Modeling. *Separation and Purification Technology*. <https://doi.org/10.1016/j.seppur.2017.01.007>
- Calzadilla, W., Espinoza, L. C., Diaz-Cruz, M. S., Sunyer, A., Aranda, M., Peña-Farfal, C., & Salazar, R. (2021). Simultaneous degradation of 30 pharmaceuticals by anodic oxidation: Main intermediaries and by-products. *Chemosphere*, 269(XXXX). <https://doi.org/10.1016/j.chemosphere.2020.128753>
- Cruz-Díaz, M. R., Rivero, E. P., Rodríguez, F. A., & Domínguez-Bautista, R. (2018). Experimental study and mathematical modeling of the electrochemical degradation of dyeing wastewaters in presence of chloride ion with dimensional stable anodes (DSA) of expanded meshes in a FM01-LC reactor. *Electrochimica Acta*, 260(2018), 726–737. <https://doi.org/10.1016/j.electacta.2017.12.025>
- Deborde, M., & von Gunten, U. (2008). Reactions of chlorine with inorganic and organic compounds during water treatment-Kinetics and mechanisms: A critical review. *Water Research*, 42(1–2), 13–51. <https://doi.org/10.1016/j.watres.2007.07.025>
- Du, X., Zhang, K., Xie, B., Zhao, J., Cheng, X., Kai, L., Nie, J., Wang, Z., Li, G., & Liang, H. (2019). Peroxymonosulfate-assisted electro-oxidation/coagulation coupled with ceramic membrane for manganese and phosphorus removal in surface water. *Chemical Engineering Journal*, 365(January), 334–343. <https://doi.org/10.1016/j.cej.2019.02.028>
- Feng, Y., Yang, L., Liu, J., & Logan, B. E. (2016). Electrochemical technologies for wastewater treatment and resource reclamation. *Environmental Science: Water Research and Technology*, 2(5), 800–831. <https://doi.org/10.1039/c5ew00289c>
- García-Espinoza, J. D., & Nacheva, P. M. (2019). Degradation of pharmaceutical compounds in water by oxygenated electrochemical oxidation: Parametric optimization, kinetic studies and toxicity assessment. *Science of the Total Environment*, 691, 417–429. <https://doi.org/10.1016/j.scitotenv.2019.07.118>
- Govindan, K., Raja, M., Noel, M., & James, E. J. (2014). Degradation of pentachlorophenol by hydroxyl radicals and sulfate radicals using electrochemical activation of peroxomonosulfate, peroxodisulfate and hydrogen peroxide. *Journal of Hazardous Materials*, 272, 42–51. <https://doi.org/10.1016/j.jhazmat.2014.02.036>
- Kobyas, M., Gengec, E., & Demirbas, E. (2016). Operating parameters and costs assessments of a real dyehouse wastewater effluent treated by a continuous electrocoagulation process. *Chemical Engineering and Processing - Process Intensification*, 101, 87–100. <https://doi.org/10.1016/j.cep.2015.11.012>

- Lan, Y., Coetsier, C., Causserand, C., & Groenen Serrano, K. (2017). On the role of salts for the treatment of wastewaters containing pharmaceuticals by electrochemical oxidation using a boron doped diamond anode. *Electrochimica Acta*, 231, 309–318. <https://doi.org/10.1016/j.electacta.2017.01.160>
- Ling, L., Zhang, D., Fan, C., & Shang, C. (2017). A Fe(II)/citrate/UV/PMS process for carbamazepine degradation at a very low Fe(II)/PMS ratio and neutral pH: The mechanisms. *Water Research*, 124(I), 446–453. <https://doi.org/10.1016/j.watres.2017.07.066>
- Liu, Y. J., Hu, C. Y., & Lo, S. L. (2019). Direct and indirect electrochemical oxidation of amine-containing pharmaceuticals using graphite electrodes. *Journal of Hazardous Materials*, 366(December 2018), 592–605. <https://doi.org/10.1016/j.jhazmat.2018.12.037>
- Luna-Trujillo, M., Palma-Goyes, R., Vazquez-Arenas, J., & Manzo-Robledo, A. (2020). Formation of active chlorine species involving the higher oxide MO_x+1 on active Ti/RuO₂-IrO₂ anodes: A DEMS analysis. *Journal of Electroanalytical Chemistry*, 878, 114661. <https://doi.org/10.1016/j.jelechem.2020.114661>
- Martínez-Sánchez, C., Robles, I., & Godínez, L. A. (2022). Review of recent developments in electrochemical advanced oxidation processes: application to remove dyes, pharmaceuticals, and pesticides. In *International Journal of Environmental Science and Technology* (Issue 0123456789). Springer Berlin Heidelberg. <https://doi.org/10.1007/s13762-021-03762-9>
- Mijin, D. Ž., Avramov Ivić, M. L., Onjia, A. E., & Grgur, B. N. (2012). Decolorization of textile dye CI Basic Yellow 28 with electrochemically generated active chlorine. *Chemical Engineering Journal*, 204–205, 151–157. <https://doi.org/10.1016/j.cej.2012.07.091>
- Murrieta, M. F., Brillas, E., Nava, J. L., & Sirés, I. (2020). Photo-assisted electrochemical production of HClO and Fe²⁺ as Fenton-like reagents in chloride media for sulfamethoxazole degradation. *Separation and Purification Technology*, 250, 117236. <https://doi.org/10.1016/j.seppur.2020.117236>
- Palma-Goyes, R. E., Vazquez-Arenas, J., Ostos, C., Ferraro, F., Torres-Palma, R. A., & Gonzalez, I. (2016). Microstructural and electrochemical analysis of Sb₂O₅ doped-Ti/RuO₂-ZrO₂ to yield active chlorine species for ciprofloxacin degradation. *Electrochimica Acta*, 213, 740–751. <https://doi.org/10.1016/j.electacta.2016.07.150>
- Qiong, Y., Jin, G., Zhou, Q., Ning, H., Yan, Y., Nai, R., & Gao, Y. (2021). Electrochemically activated peroxymonosulfate for the abatement of chloramphenicol in water : performance and mechanism. *Environmental Science and Pollution Research*, 0123456789. <https://doi.org/10.1007/s11356-021-17089-y>
- Rodriguez-Narvaez, O. M., Pacheco-Alvarez, M. O. A., Wróbel, K., Páramo-Vargas, J., Bandala, E. R., Brillas, E., & Peralta-Hernandez, J. M. (2020). Development of a Co²⁺/PMS process involving target contaminant degradation and PMS decomposition. *International Journal of Environmental Science and Technology*, 17(1), 17–26. <https://doi.org/10.1007/s13762-019-02427-y>
- Santos, D. H. S., Duarte, J. L. S., Tavares, M. G. R., Tavares, M. G., Friedrich, L. C., Meili, L., Pimentel, W. R. O., Tonholo, J., & Zanta, C. L. P. S. (2020). Electrochemical degradation and toxicity evaluation of reactive dyes mixture and real textile effluent over DSA® electrodes. *Chemical Engineering and Processing - Process Intensification*, 153(April), 107940. <https://doi.org/10.1016/j.cep.2020.107940>
- Sierra-Rosales, P., Berríos, C., Miranda-Rojas, S., & Squella, J. A. (2018). Experimental and theoretical insights into the electrooxidation pathway of azo-colorants on glassy carbon electrode. *Electrochimica Acta*, 290, 556–567. <https://doi.org/10.1016/j.electacta.2018.09.090>

- Soni, B. D., Patel, U. D., Agrawal, A., & Ruparelia, J. P. (2020). Electrochemical destruction of RB5 on Ti/PtOx–RuO2–SnO2–Sb2O5 electrodes: a comparison of two methods for electrode preparation. *International Journal of Environmental Science and Technology*, 17(2), 903–916. <https://doi.org/10.1007/s13762-019-02393-5>
- Sravanth, T., Ramesh, S. T., Gandhimathi, R., & Nidheesh, P. V. (2020). Continuous treatability of oily wastewater from locomotive wash facilities by electrocoagulation. *Separation Science and Technology (Philadelphia)*, 55(3), 583–589. <https://doi.org/10.1080/01496395.2019.1567548>
- Stupar, S. L., Grgur, B. N., Radišić, M. M., Onjia, A. E., Ivanković, N. D., Tomašević, A. V., & Mijin, D. (2020). Oxidative degradation of Acid Blue 111 by electro-assisted Fenton process. *Journal of Water Process Engineering*, 36(November 2019). <https://doi.org/10.1016/j.jwpe.2020.101394>
- Szpyrkowicz, L., Juzzolino, C., Kaul, S. N., Daniele, S., & Faveri, M. D. De. (2000). Electrochemical Oxidation of Dyeing Baths Bearing Disperse Dyes. *Industrial and Engineering Chemistry Research*, 39, 3241–3248.
- Szpyrkowicz, L., Radaelli, M., Daniele, S., Baldacci, A., & Kaul, S. (2007). Application of electrocatalytic mediated oxidation for the treatment of a spent textile bath in a membrane reactor. *Industrial and Engineering Chemistry Research*, 46(21), 6732–6736. <https://doi.org/10.1021/ie0616388>
- Tamura, H., Goto, K., Yotsuyanagi, T., & Nagayama, M. (1974). Spectrophotometric determination of iron(II) with 1,10-phenanthroline in the presence of large amounts of iron(III). *Talanta*, 21(4), 314–318. [https://doi.org/10.1016/0039-9140\(74\)80012-3](https://doi.org/10.1016/0039-9140(74)80012-3)
- Vijayakumar, S., Chen, J., Amarnath, M., Tungare, K., Bhorl, M., Divya, M., González-Sánchez, Z. I., Durán-Lara, E. F., & Vaseeharan, B. (2021). Cytotoxicity, phytotoxicity, and photocatalytic assessment of biopolymer cellulose-mediated silver nanoparticles. *Colloids and Surfaces A: Physicochemical and Engineering Aspects*, 628(July), 0–1. <https://doi.org/10.1016/j.colsurfa.2021.127270>
- Wang, H., Shen, Y., Lou, Z., Zhu, N., Yuan, H., & Liu, C. (2019). Hydroxyl radicals and reactive chlorine species generation via E⁺-ozonation process and their contribution for concentrated leachate disposal. *Chemical Engineering Journal*, 360, 721–727. <https://doi.org/10.1016/j.cej.2018.11.213>
- Wang, Y. R., & Chu, W. (2011). Degradation of a xanthene dye by Fe(II)-mediated activation of Oxone process. *Journal of Hazardous Materials*, 186(2–3), 1455–1461. <https://doi.org/10.1016/j.jhazmat.2010.12.033>
- Xiang, Q., Nomura, Y., Fukahori, S., Mizuno, T., Tanaka, H., & Fujiwara, T. (2019). Innovative Treatment of Organic Contaminants in Reverse Osmosis Concentrate from Water Reuse: a Mini Review. *Current Pollution Reports*, 5(4), 294–307. <https://doi.org/10.1007/s40726-019-00119-2>
- Xiang, Y., Fang, J., & Shang, C. (2016). Kinetics and pathways of ibuprofen degradation by the UV/chlorine advanced oxidation process. *Water Research*, 90, 301–308. <https://doi.org/10.1016/j.watres.2015.11.069>
- Yang, N., Cui, J., Zhang, L., Xiao, W., Alshawabkeh, N., & Mao, X. (2015). Iron electrolysis-assisted peroxymonosulfate chemical oxidation for the remediation of chlorophenol-contaminated groundwater. *February*. <https://doi.org/10.1002/jctb.4659>